Lab on a Chip

Cite this: *Lab Chip*, 2012, **12**, 3968–3975

www.rsc.org/loc

PAPER

Concentration gradient generation of multiple chemicals using spatially controlled self-assembly of particles in microchannels†‡

Eunpyo Choi,[a] Hyung-kwan Chang,[a] Chae Young Lim,[a] Taesung Kim[b] and Jungyul Park*[a]

Received 30th April 2012, Accepted 31st July 2012
DOI: 10.1039/c2lc40450h

We present a robust microfluidic platform for the stable generation of multiple chemical gradients simultaneously using *in situ* self-assembly of particles in microchannels. This proposed device enables us to generate stable and reproducible diffusion-based gradients rapidly without convection flow: gradients are stabilized within 5 min and are maintained steady for several hours. Using this device, we demonstrate the dynamic position control of bacteria by introducing the sequential directional change of chemical gradients. Green Fluorescent Protein (GFP)-expressing bacterial cells, allowing quantitative monitoring, show not only tracking motion according to the directional control of chemical gradients, but also the gradual loss of sensitivity when exposed to the sequential attractants because of receptor saturation. In addition, the proposed system can be used to study the preferential chemotaxis assay of bacteria toward multiple chemical sources, since it is possible to produce multiple chemical gradients in the main chamber; aspartate induces the most preferential chemotaxis over galactose and ribose. The microfluidic device can be easily fabricated with a simple and cost effective process based on capillary pressure and evaporation for particle assembly. The assembled particles create uniform porous membranes in microchannels and its porosity can be easily controlled with different size particles. Moreover, the membrane is biocompatible and more robust than hydrogel-based porous membranes. The proposed system is expected to be a useful tool for the characterization of bacterial responses to various chemical sources, screening of bacterial cells, synthetic biology and understanding many cellular activities.

Introduction

Cell migration plays essential roles in angiogenesis,[1,2] embryonic development,[3] wound healing[4–6] and cancer metastasis,[7] and it is often meditated by a chemical gradient.[8] Therefore, many types of devices have been developed for chemotaxis study. The first quantitative chemotaxis assay was the capillary assay, developed by Adler in 1960s,[9] and the Boyden chamber and the Dunn chamber which were developed and commonly used as standard chemotaxis assays.[10] Recently, microfluidic devices show high potential in studying cell migration, because they provide *in vitro* environments that are similar to *in vivo* environments.[11] To date, the developed microfluidic devices for chemical gradient generation can be categorized into convection flow-based and diffusion-based methods.[12] The convection flow-based methods show a unique advantage over diffusion-based methods in that they can generate controllable and switchable gradients.[13] However, the convection flow can sweep away secreted biomolecules from cells, and viscous shear stresses from the flow interfere with the cell migration—especially swimming cells like bacteria. Therefore, for bacterial chemotaxis study, diffusion-based gradient generation is more suitable. Basically, diffusion-based gradient generation utilizes porous membranes, such as polyethylene, polycarbonate and hydrogels. Since hydrogels allow similar diffusion conditions to water, various microfluidic devices based on hydrogel membranes have been developed.[14–17] Nevertheless, current hydrogel-based membranes have some drawbacks. For example, the agarose-based microfluidic device is constructed with stacks of many layers (*e.g.*, agarose membrane, PDMS spacer, glass slide and stainless steel) and it can induce fluid leakage. Photopolymerizable hydrogels can form a porous membrane in the desired shape and position within a few seconds, but they require extra photoemission equipment and have cytotoxic photo-initiators.[18] The most critical problem of hydrogels is that hydrogels are not robust without an aqueous environment and change their volume according to the level of water absorption.

Recently, some studies have been reported about the diffusion-based method, which can realize the generation of multiple

[a]*Department of Mechanical Engineering, Sogang University, Sinsu-dong, Mapo-gu, Seoul, 121-742, Korea. E-mail: sortpark@sogang.ac.kr; Fax: +82-2-712-0799; Tel: +82-2-705-8642*
[b]*School of Mechanical and Advanced Materials Engineering, Ulsan National Institute of Science and Technology, UNIST-gil 50, Eonyang-eup, Ulsan, 689-798, Korea*
† Published as part of a themed issue dedicated to Emerging Investigators
‡ Electronic Supplementary Information (ESI) available. See DOI: 10.1039/c2lc40450h

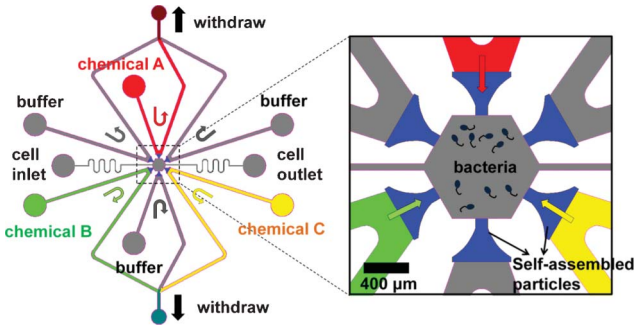

Fig. 1 A schematic view of the configuration and principle idea. Each channel connected with the center chamber is isolated by porous membranes formed with the self-assembled particles. Nano-interstices in the closed-packed particles realize the stable chemical gradients without any external flow disturbance. All channels are filled with buffer and different chemicals are introduced into channels. Subsequently, in order to constantly maintain the concentration in each channel, the flows are withdrawn carefully. Chemicals are diffused through the membrane and stable gradients are generated in the center chamber.

chemical gradients.[19–22] However, in some cases it is not easy to fabricate the devices because they are composed with complex multilayered microfluidic parts.[19,20,22] Also, in other cases, it is hard to have spatio-temporal control of the chemical gradient direction.[21]

In order to overcome these drawbacks, we propose diffusion-based multiple chemical gradient generation using *in situ* self-assembly of polystyrene particles in microchannels. Fig. 1 shows the configuration and principle idea of the proposed microfluidic device. There exist source channels to supply the molecules to the center chamber, and on the right opposite side, there are sink channels to remove the same quantities of molecules from the center chamber. Moreover, the center chamber is fully separated from the source and sink channels by the diffusible porous membrane, which is formed by nano-interstices of self-assembled polystyrene particles. Therefore, if 100% and 0% of concentration is introduced by withdrawing the flow at the source and sink channels, respectively, stable chemical gradients can be preserved in the center chamber without any external flow disturbance. This proposed polystyrene particle-based membrane device has several advantages. (1) It can be simply fabricated with only one PDMS layer and needs simple microfluidic handling without any external heavy equipment. The shape and position of the assembled particles are manipulated easily by controlling capillary pressure. (2) The porosity of the membrane can be adjusted by using a different size of particles. (3) Also, polystyrene itself is non-cytotoxic to the bacterial cells[23,24] and robust in a dry environment, so that it can be kept for a longer term than a hydrogel-based membrane. Generally, a hydrogel-based membrane should be fabricated just before bacterial chemotaxis study and the biologist may not easily handle the device.

Moreover, using the proposed device, chemical gradients are stabilized within a short time (<5 min) and maintained for several hours for small molecules (with a diffusion coefficient of approximately 10^{-9} m^2 s^{-1}). Owing to the fast and stable gradient generation, this is very useful in chemotactic studies of bacterial cells (GFP expressing *Salmonella typhimurium*). This useful ability is proved by demonstrating dynamic position control of bacteria by introducing the sequential directional change of chemical gradients. Also, we demonstrate that the proposed system can be applied to the study of the preferential chemotaxis assay of bacteria when exposed to multiple chemical sources because cells in *in vivo* environments are exposed to various attractants and stimulants simultaneously. For examples, multiple biochemical signals are required to direct the recruitment of leukocytes into tissues, which is relevant for all instances of inflammation.[25,26] Therefore, we believe that the device will be a useful tool for characterizing bacterial responses to various chemical sources, screening bacterial cells, synthetic biology and understanding many cellular activities.

Materials and methods

Fabrication process of PDMS microfluidic channel

The PDMS microfluidic chip was fabricated using the standard soft lithography. Details for the fabrication process are provided in Fig. S1, ESI‡. Briefly, Fig. S1(a–e)‡ shows the fabrication process with the multilayered design: (a) A 4 inch silicon wafer was patterned with SU-8 resist. The height of the first layer for the shallow channel that can form the desired patterns for the porous membrane is approximately 5 μm. (b) Subsequently, SU-8 2050 was patterned on the first SU-8 layer (target: 100 μm, this layer is for the deep channel) (c) The PDMS mixture was poured onto the master and cured at 95 °C for 1 h. (d) The PDMS was then peeled off. (e) Finally, it was bonded with a slide glass after O_2 plasma treatments.

In situ formation of porous membrane

Fig. 2 shows the fabrication process for the *in situ* formation of porous membranes using the self-assembly of particles within the PDMS channel. The PDMS device with shallow and deep channels was fabricated as described above (Fig. 2(a)). In this paper, we used the diameter 3.524 μm of carboxylated polystyrene microspheres (standard deviation: 0.119 μm, Polyscience Inc., Warrington, USA). Firstly, 100 μL of the diluted microspheres (1.68×10^8 particles) were centrifuged at 10 000 rpm for 1 min and resuspended in 100 μL of 70% ethanol (v/v). Finally, 2 μL (0.03×10^8 particles) of this solution was introduced into the deep channels by capillary pressure (Fig. 2(b)). The diluted microspheres at the intersection between the shallow and deep channels experience a sudden pressure drop (ΔP_{12}), which tries to drag the solution in the deep channel into the shallow channel ($F_{shallow}$) (Fig. 2(c)).[27] In the designed horn-shaped channel, since more evaporation and capillary pressure were induced at the narrow opening, all particles were moved toward the narrow opening. However, the diluted microspheres could not move forward at the interface between the narrow opening and the expansion channel (center chamber) because the capillary stop pressure was maximized at the expansion angle β around 90° (Fig. 2(d, e)).[28] During this time, the solution was dried out, microspheres were self-assembled unidirectionally, and nanopores were formed from nano-interstices in these closed-packed microspheres, only within the shallow channel (Fig. 2(f)). Finally, we annealed the self-assembled particles for 1 h at 90 °C.

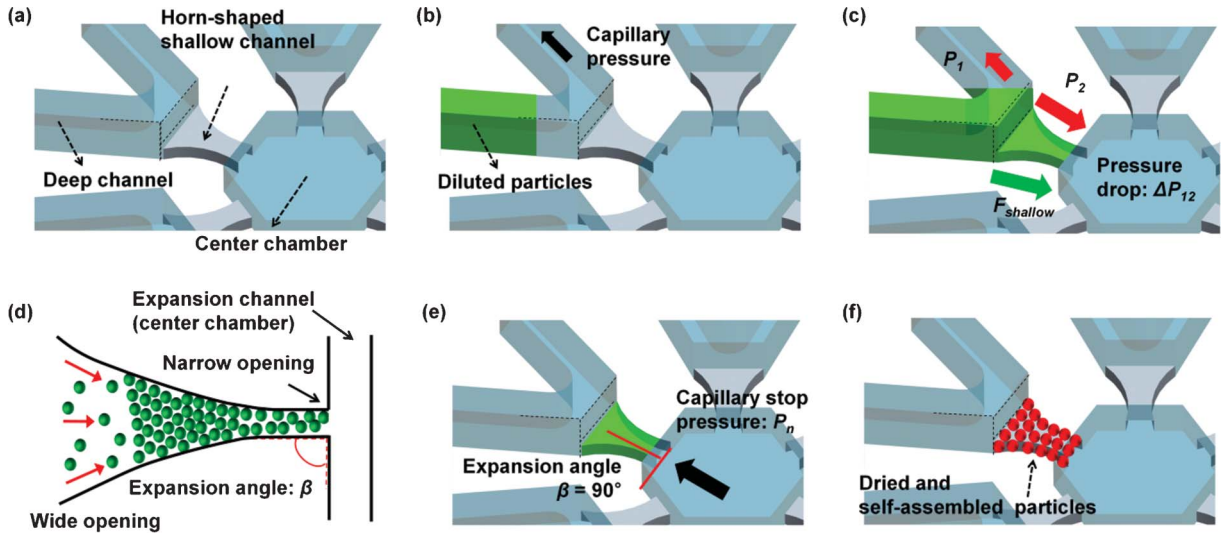

Fig. 2 The fabrication process for the *in situ* formation of the nanoporous membranes within the PDMS channels: (a) The PDMS device with shallow and deep channels was molded from a SU-8 resist master with two different heights. (b) Diluted nanoparticles were introduced into the deep channels by capillary pressure. (c) The diluted nanoparticles at the intersection between the shallow and deep channels experience a sudden pressure drop, which tries to drag the solution in the deep channel into the shallow channel. (d, e) In the designed horn-shaped channel, since more evaporation and capillary pressure are induced at the narrow opening, the crystallization was formed unidirectionally. The solution could not move over the interface between the narrow-opening and the expansion channel during the crystallization because of the capillary stop valve. (f) During this time, the solution was dried out and nanoparticles were self-assembled within the shallow channel.

Preparation of bacteria cells

Engineered attenuated *Salmonella typhimurium* defective in guanosine 5′-diphosphate-3′-diphosphate (ppGpp) synthesis (ΔppGpp strain) used to express the bacterial luciferase gene lux for generating imaging signals was used in a chemotaxis experiment.[29] Cells were cultured overnight in 5 mL of Luria–Bertani (LB) medium (Fisher, Pittsburgh, PA, USA) supplemented with 50 μg mL^{-1} ampicillin and kanamycin at 37 °C in an incubator with shaking at 200 rpm. A 1% culture of the bacterial solution in LB medium containing ampicillin and kanamycin was prepared. Then, cells were incubated in a shaking incubator (37 °C, 200 rpm) for 3 to 4 h until the 600 nm optical density (OD_{600}) of the cell culture reached 1.0. Finally, the cells were centrifuged at 3000 rpm at room temperature and resuspended in M9 medium (minimal salt, BD, NJ, USA. In all experiments, we used M9 medium as a base solution containing the 10^{-3} M of glucose). Before cells were loaded, the center chamber was coated with Pluronic surfactant (F-127, 1%, Sigma-Aldrich, St. Louis, MO, USA) to minimize any nonspecific binding between the cells and the glass surface over 2 h and was subsequently rinsed with M9 medium. Finally, a 1 μL drop of prepared cell suspension was loaded into the center chamber.

Experimental setup and data analysis

In this study, we used 50 μM of the FITC (fluorescein isothiocyanate), Dylight 549 and Rhodamine B fluorescence dye based on M9 medium in order to characterize the proposed microfluidic device. The diffusivity of FITC (MW 389), rhodamine B (MW 444) and Dylight549 (MW 1040) in water at room temperature was assumed to be 0.49×10^{-9} m^2 s^{-1}, 0.45×10^{-9} m^2 s^{-1} and 0.38×10^{-9} m^2 s^{-1}, respectively.[17,30,31] We used the α-methyl-DL-aspartic acid (Sigma-Aldrich, St. Louis, MO, USA) based on M9 medium as a chemo-attractant for spatio-temporal control experiments. For experiments about the preferential chemotaxis toward multiple chemo-attractants, we used the same molarity of the α-methyl-DL-aspartic acid, D-galactose (Daejung Chemicals & Metals, Shiheung-City, Korea) and D-ribose (Sigma-Aldrich) based on M9 medium. The diffusion coefficient of α-methyl-DL-aspartic acid (MW 147.13), D-galactose (MW 180.16) and D-ribose (MW 150.13) in water at room temperature was assumed to be 0.90×10^{-9} m^2 s^{-1}, 0.70×10^{-9} m^2 s^{-1} and 0.77×10^{-9} m^2 s^{-1}, respectively.[32–34] The fluorescence intensities could be quantitatively assessed from the captured images using ImagePro Plus (MediaCybernetics, Bethesda, MD, USA) software. A precise microsyringe pump (NE-1000, New Era Pump System, USA) was employed to control the flow rate in the microchannel through the microtubes. All of the studies were monitored using an inverted microscope (IX7, Olympus Co., Tokyo, Japan) and images were captured on a PC using a CCD camera (CoolSNAP, Photometrices, Tucson, AZ, USA) installed in the microscope.

To quantify the cell count, GFP-expressing cells at different normalized concentrations (0.2, 0.4, 0.6, 0.8 and 1.0) were loaded into the open-cylinder type reservoir with 900 μm diameter and the fluorescence signals were used to calibrate cell count (see more details in chapter S.2, ESI‡). Moreover, tracked trajectories for bacterial cells were analyzed using ImagePro Plus and all graphs were drawn using Sigmaplot 9.0 (Jandel Scientific, San Rafael, CA, USA).

Results and discussions

Device characterization

The photograph of the fabricated PDMS microfluidic channels with porous membranes is shown in Fig. 3(a), and Fig. 3(b)

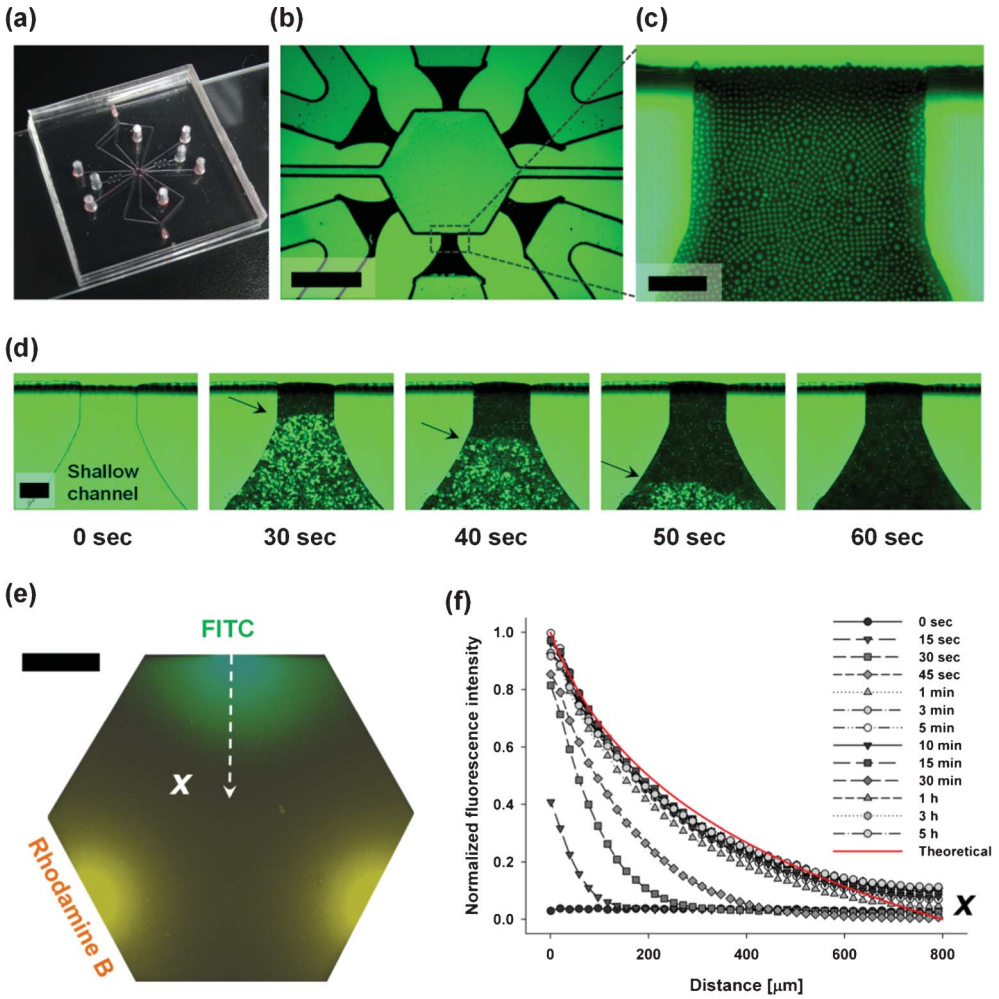

Fig. 3 (a) The photograph of the fabricated PDMS microfluidic channels (b) A microscopy image of the center chamber (scale bar: 400 μm). (c) Enlarged microscopy images of self-assembled microspheres (scale bar: 25 μm) at the interface between the narrow opening and the expansion channel (center chamber). (d) Time sequence images of particle self-assembly within a shallow channel. (e) Overlapping fluorescence images of three different fluorescence dyes at steady-state (scale bar: 200 μm). (f) Corresponding normalized fluorescence intensity plots. Steady-state gradients were established within 5 min.

depicts the microscopy image of the center chamber (scale bar: 400 μm). Each channel connected with the center chamber is isolated by the porous membranes formed with the self-assembled microspheres. Fig. 3(c) shows the enlarged microscopy images (scale bar: 25 μm) of the interface between the narrow opening and the expansion channel (center chamber). As shown in Fig. 3(d), the assembly of particles was formed unidirectionally and diluted microspheres could not move forward at the interface between the narrow opening and the expansion channel during evaporation of the medium (scale bar: 50 μm). During this time, the solution was dried out and microspheres were self-assembled with an ideal FCC (face centered cubic) package only within the shallow channel. Nano-interstices in these close-packed microsphere lattices create a diffusible membrane that consists of voids interconnected by narrower pores, which have an equivalent diameter ~15% of the sphere size.[35] It took about 60 s to fully assemble microspheres within the shallow channel (see movie S1 in the ESI‡, images were acquired at a rate of 30 frames min^{-1}).

We tested the permeability of the membrane using fluorescence dyes. Three different fluorescence dyes were introduced into each source channel at 90° for FITC, 210° for Rhodamine B and 330° for Dylight 549. Subsequently, in order to maintain the solution concentration, a flow rate of 4.0 μL min^{-1} was controlled by withdrawing the solution. Finally, M9 medium was introduced into the center chamber. Since there is no net flow of M9 medium in the center channel, but the permeation of fluorescence dyes through the membranes occurs, a stable concentration is established across the center channel and its overlapping fluorescence images at steady-state are shown in Fig. 3(e) (scale bar: 200 μm). Fig. 3(f) shows one of the representative plots of the normalized FITC (90°) fluorescence intensity profiles across the center channel as a function of time. Steady-state gradients were established within 5 min and maintained for several hours. Theoretically, the gradient will be stable indefinitely, but there was a slight drift in the concentration curves from 15 min to 5 h. It seems that there might be a little evaporation from the center chamber through the PDMS due to its porosity. Nevertheless, the proposed device

is very useful in this chemotactic study of bacterial cells because all experiments will be done within 15 min.

Moreover, the decay in fluorescent intensity along the membrane was observed, as shown in Fig. S3, ESI‡. When we used FITC, there was a 50% intensity gap between the source channel and center chamber after 1 h and this result shows that the real concentration of chemo-attractant at the center chamber might be lower than the source channel.

The theoretical profile (red line) of fluorescence evolution in Fig. 3(f) was obtained from the time-dependent (t) solution of the diffusion equation in two-dimensions.[36] In our proposed device, since the chemical molecules were diffused through the radial direction, it is more practical to use a circular cylindrical coordinate. Therefore, in fixed boundary conditions, the diffusion equation can be derived as follows (more details are in section S.4, ESI‡):

$$C = \frac{C_1 \ln(b/r) + C_2 \ln(r/a)}{\ln(b/a)} \quad (1)$$

where C_1 is the initial concentration at $r = a$ and its value is 1, and C_2 is the final concentration at $r = b$ and its value is 0 (a and b are the initial and final position at the center chamber, respectively). Finally, in steady-state, the theoretical solution showed a good agreement with experimental results.

Moreover, this established steady-state time could be easily controlled by using a different pore size of the membrane. Fig. S4‡ shows the time evolution fluorescence profiles using 300 $\pm$ 15 nm silica nanoparticles and, with this condition, the steady-state gradients were established within 20 min.

Spatio-temporal control

The movement control of *Salmonella typhimurium* was demonstrated by sequentially introducing the chemo-attractants (aspartate) and observing the movement depending on the direction of chemical gradients (Fig. 4).

First, in order to find the strongest chemotactic response toward the aspartate, experiments were repeated with five different concentrations ranging from 10^{-4} M to 1 M. The aspartate was introduced into the source channel at 90° and M9 medium was introduced at the others. Then, to maintain the solution concentration in the source and sink channels, a flow rate of 4.0 μL min^{-1} was controlled by withdrawing the solution. Finally, bacteria cells were loaded into the center chamber and images were acquired until 15 min and, using the calibration data in Table S1 in ESI‡, the number of cells was quantified. As shown in Fig. S5 in ESI‡, the strongest response for aspartate was found in the presence of 10^{-1} M concentration gradient.

As shown in Fig. 4(a) and (b), tracked trajectories for *Salmonella typhimurium* migrating in a chemical gradient with 10^{-1} M of aspartate were analyzed. The trajectories were obtained from 10 s sequence images at the middle of the center chamber and these trajectories were plotted with each of the tracks originating at the center. Right after the cells were loaded (Fig. 4(a)), they execute a run and tumble mode, so that no biased migration is observed. However, 120 s after the cells were loaded, they showed positive chemotaxis toward the higher aspartate gradient (90°) with a run mode rather than a tumble mode (Fig. 4(b)).

Using the above chemotactic response results of *Salmonella typhimurium*, the spatio-temporal controlling was performed. Every 180 s, the 10^{-1} M of the aspartate was sequentially introduced into the source channel at 210°, 330°, and 90° in this order and images were acquired at a rate of 2 frames min^{-1}. Fig. 4(c) shows time sequence fluorescence images of the GFP expressing *Salmonella typhimurium* (scale bars: 200 μm). The fluorescence intensities were increased sequentially where the aspartate was introduced and it means that bacterial cells sensed the change of the environment and they responded toward the higher aspartate gradient (see movie S2 in ESI‡). The experiments were performed more than 10 times and the representative average polar plot with the quantified number of cells and a vertical bar plot with error bars (standard deviation) especially at 210° (180 s), 330° (360 s), and 90° (540 s) were drawn, as shown in Fig. 4(d) and (e), respectively. These plots indicate that the spatio-temporal control of *Salmonella typhimurium* was well performed, but the number of cells showing the chemotactic response decreased gradually as the direction of the chemo-attractant gradient changed. The decrement of the response sensitivity could be explained by the reports that repeated exposure of the same chemo-attractants may lead to the saturation of the adaptation rate because the number of chemo-receptors in cell membranes is limited.[9,37,38]

Preferential chemotaxis of bacteria cells toward multiple chemo-attractants

The experiment for the preferential chemotaxis of *Salmonella typhimurium* toward three different chemo-attractants (aspartate, ribose and galactose) was demonstrated because bacterial cells are known to have chemo-receptors, such as *tar* for aspartate and *trg* for ribose and galactose, *etc.*[39,40]

Aspartate, galactose and ribose at the same molarity were introduced into the each different source channel at 90°, 210° and 330°, respectively. Subsequently, in order to maintain the solution concentration in the source and sink channels, a flow rate of 4.0 μL min^{-1} was controlled by withdrawing the solution. Finally, bacteria cells were loaded into the center chamber and images were acquired. Fig. 5(a) and (b) show tracked trajectories for bacteria cells migrating in a chemical gradient with 10^{-1} M of three different chemo-attractants. The trajectories were obtained in the same manner as Fig. 4(a) and (b). Right after the cells were loaded, the bacterial cells execute a run and tumble mode, but no biased migration was observed, as shown in Fig. 5(a). However, 120 s later, cells sensed a change in the chemical environment and most cells migrated toward the higher aspartate gradient with a run mode rather than a tumble mode (Fig. 5(b)).

As shown in the time sequence fluorescence images (Fig. 5(c)) and movie S3 in ESI‡, the GFP-expressing *Salmonella typhimurium* showed strong positive chemotaxis toward aspartate, but it was hard to observe chemotactic responses in the galactose and ribose gradients. Furthermore, by quantifying the number of cells, *Salmonella typhimurium* seems more sensitive to the aspartate than galactose and ribose, as shown in Fig. 5(d) and (e). These results show good agreement with other previous reports that *Salmonella typhimurium* have a stronger response to the aspartate than other chemo-attractants; for *Salmonella typhimurium* the strongest ribose response is 10 times less than

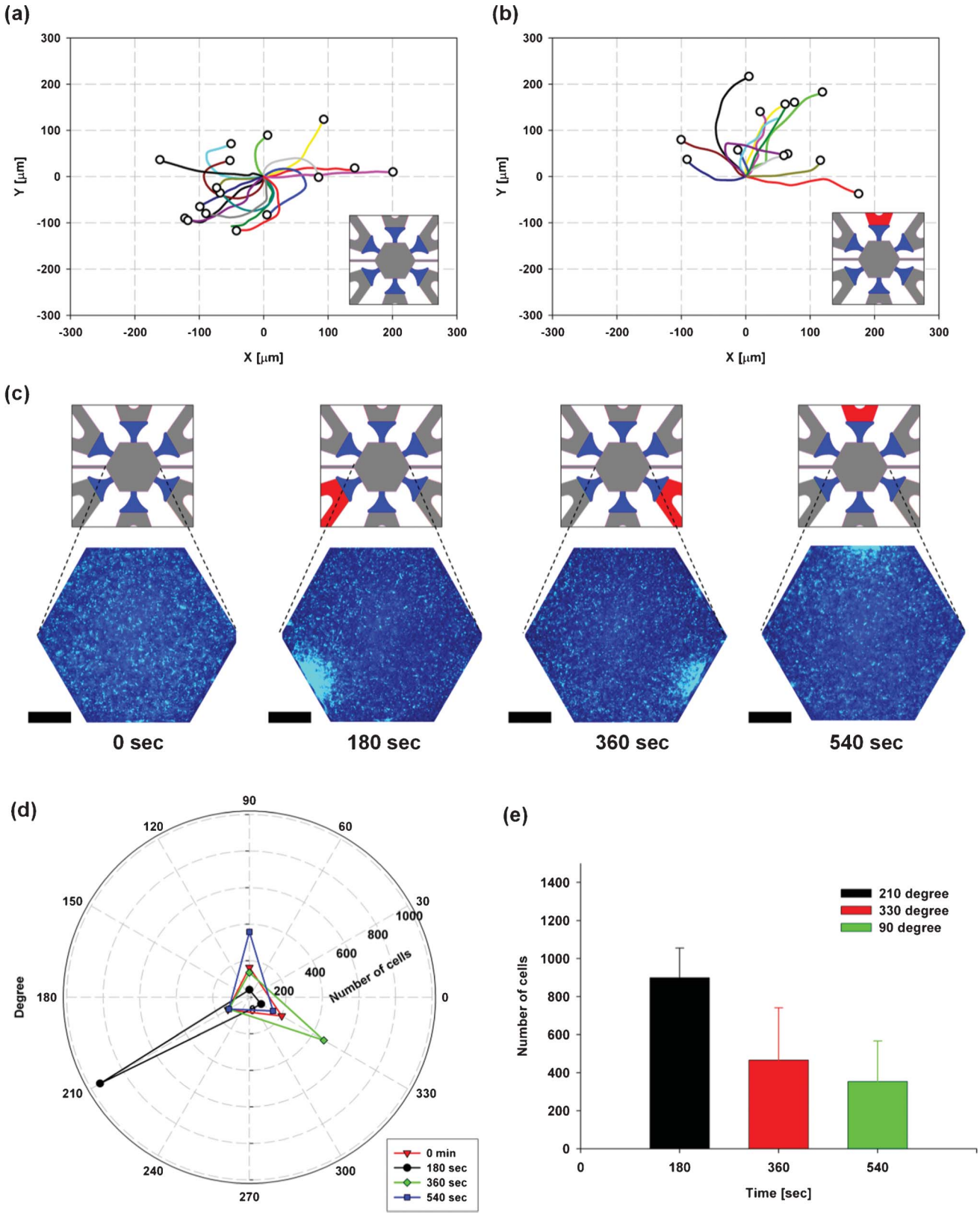

Fig. 4 (a) Tracked trajectories of *Salmonella typhimurium* migrating right after they were loaded and (b) 120 s later. (c) Time sequence fluorescence images of the spatio-temporally controlled cells (scale bars: 200 μm). (d) One of the representative average polar plots with the quantified number of cells. (e) Vertical bar plots with error bars (standard deviation) especially at 210° (180 s), 330° (360 s), and 90° (540 s).

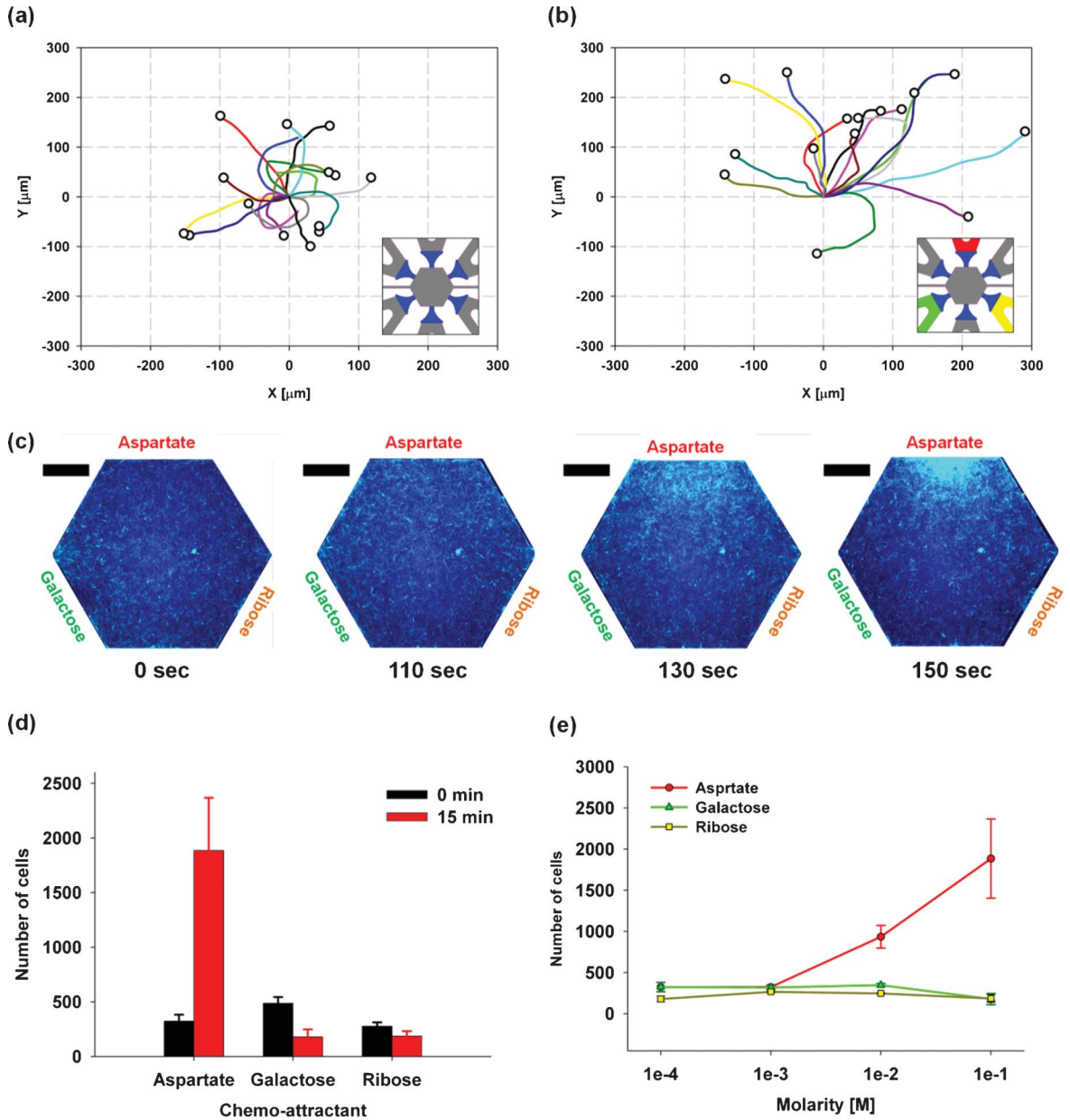

Fig. 5 The experiment for the preferential chemotaxis assay of *Salmonella typhimurium* toward three different chemo-attractants. (a) Tracked trajectories of *Salmonella typhimurium* migrating right after they were loaded and (b) 120 s later. (c) Time sequence fluorescence images of the GFP-expressing *Salmonella typhimurium* in the multiple chemical gradients (scale bars: 200 μm). (d) A vertical bar plot of the quantified number of cells with error bars (standard deviation). *Salmonella typhimurium* seems more sensitive to the aspartate than the galactose and the ribose. (e) Chemotactic responses toward different concentrations.

the strongest aspartate response[41,42] and ribose has a similar response to galactose.[43,44]

Conclusions

We developed a robust gradient generator of multiple chemicals using self-assembled particles in microchannels. The porous membranes based on the assembled particles allow fast and stable gradient generation without any convection flow disturbance and leakage, they are more robust in a dry environment and have long-term storage potential compared to hydrogel-based membranes. Dynamic spatial control of bacterial cells was successfully demonstrated by changing the direction of chemical gradients every 180 s. In addition, bacterial cells tracked the dynamic change of chemical gradients, but gradually became insensitive to the repeated exposure of the same attractants due to the saturation of chemo-receptors. Using the proposed system, the parallel preferential chemotaxis assay was performed. *Salmonella typhimurium* showed stronger positive chemotaxis toward aspartate than galactose and ribose. We believe that our proposed system can be a useful tool for parallel and rapid characterization of bacterial responses to various chemical sources, screening of bacterial cells, synthetic biology and understanding many cellular activities.

Acknowledgements

We wish to thank Jung-Joon Min in Chonnam National University for providing strained bacteria and Jinwon Lee in Sogang University for help with culturing the bacteria. This work was supported by the Pioneer Research Center Program ''Bacteriobot'' through the National Research Foundation of Korea funded by the Ministry of Education, Science and Technology (2009-0082953).

References

1 S. Chung, R. Sudo, V. Vickerman, I. K. Zervantonakis and R. D. Kamm, *Ann. Biomed. Eng.*, 2010, **38**, 1164–1177.
2 J. Bischoff, *Trends Cell Biol.*, 1995, **5**, 69–74.
3 A. J. Ridley, M. A. Schwartz, K. Burridge, R. A. Firtel, M. H. Ginsberg, G. Borisy, J. T. Parsons and A. R. Horwitz, *Science*, 2003, **302**, 1704–1709.
4 D. H. Kim, P. K. Wong, J. Park, A. Levchenko and Y. Sun, *Annu. Rev. Biomed. Eng.*, 2009, **11**, 203–233.
5 J. Park, D. H. Kim, G. Kim, Y. Kim, E. Choi and A. Levchenko, *Lab Chip*, 2010, **10**, 2130–2138.
6 H. Tavana, K. Kaylan, T. Bersano-Begey, K. E. Luker, G. D. Luker and S. Takayama, *Adv. Funct. Mater.*, 2011, **21**, 2920–2926.
7 S. Chung, R. Sudo, I. K. Zervantonakis, T. Rimchala and R. D. Kamm, *Adv. Mater.*, 2009, **21**, 4863–4867.
8 C. A. Parent and P. N. Devreotes, *Science*, 1999, **284**, 765–770.
9 J. Adler, *Science*, 1969, **166**, 1588–1597.
10 S. Toetsch, P. Olwell, A. Prina-Mello and Y. Volkov, *Integr. Biol.*, 2009, **1**, 170–181.
11 M. Kim and T. Kim, *Anal. Chem.*, 2010, **82**, 9401–9409.
12 T. Kim, M. Pinelis and M. M. Maharbiz, *Biomed. Microdevices*, 2009, **11**, 65–73.
13 D. Amarie, J. A. Glazier and S. C. Jacobson, *Anal. Chem.*, 2007, **79**, 9471–9477.
14 Y. Ling, J. Rubin, Y. Deng, C. Huang, U. Demirci, J. M. Karp and A. Khademhosseini, *Lab Chip*, 2007, **7**, 756–762.
15 S. Y. Cheng, S. Heilman, M. Wasserman, S. Archer, M. L. Shuler and M. Wu, *Lab Chip*, 2007, **7**, 763–769.
16 J. Diao, L. Young, S. Kim, E. A. Fogarty, S. M. Heilman, P. Zhou, M. L. Shuler, M. Wu and M. P. DeLisa, *Lab Chip*, 2006, **6**, 381–388.
17 E. Choi, I. Jun, H. K. Chang, K. M. Park, H. Shin, K. D. Park and J. Park, *Lab Chip*, 2012, **12**, 302–308.
18 J. Trudel and S. P. Massia, *Biomaterials*, 2002, **23**, 3299–3307.
19 J. Atencia, J. Morrow and L. E. Locascio, *Lab Chip*, 2009, **9**, 2707–2714.
20 M. Morel, J. C. Galas, M. Dahan and V. Studer, *Lab Chip*, 2012, **12**, 1340–1346.
21 C. G. Yang, Y. F. Wu, Z. R. Xu and J. H. Wang, *Lab Chip*, 2011, **11**, 3305–3312.
22 B. Mosadegh, M. Agarwal, H. Tavana, T. Bersano-Begey, Y. Torisawa, M. Morell, M. J. Wyatt, K. S. O'Shea, K. F. Barald and S. Takayama, *Lab Chip*, 2010, **10**, 2959–2964.
23 J. F. Jones, J. D. Feick, D. Imoudu, N. Chukwumah, M. Vigeant and D. Velegol, *Appl. Environ. Microbiol.*, 2003, **69**, 6515–6519.
24 M. Rosenberg, *Appl. Environ. Microbiol.*, 1981, **42**, 375–377.
25 W. Savino, D. M. Villa-Verde, D. A. Mendes-da-Cruz, E. Silva-Monteiro, A. R. Perez, P. Aoki Mdel, O. Bottasso, N. Guinazu, S. D. Silva-Barbosa and S. Gea, *Cytokine Growth Factor Rev.*, 2007, **18**, 107–124.
26 T. Sato, H. Thorlacius, B. Johnston, T. L. Staton, W. Xiang, D. R. Littman and E. C. Butcher, *J. Immunol.*, 2005, **174**, 277–283.
27 S. Chung, H. Yun and R. D. Kamm, *Small*, 2009, **5**, 609–613.
28 K. H. Chung, J. W. Hong, D. S. Lee and H. C. Yoon, *Anal. Chim. Acta*, 2007, **585**, 1–10.
29 V. H. Nguyen, H. S. Kim, J. M. Ha, Y. J. Hong, H. E. Choy and J. J. Min, *Cancer Res.*, 2010, **70**, 18–23.
30 S. A. Rani, B. Pitts and P. S. Stewart, *Antimicrob. Agents Chemother.*, 2005, **49**, 728–732.
31 P. O. Gendron, F. Avaltroni and K. Wilkinson, *J. Fluoresc.*, 2008, **18**, 1093–1101.
32 R. Jasuja, Y. Lin, D. R. Trentham and S. Khan, *Proc. Natl. Acad. Sci. U. S. A.*, 1999, **96**, 11346–11351.
33 N. Mogi, E. Sugai, Y. Fuse and T. Funazukuri, *J. Chem. Eng. Data*, 2006, **52**, 40–43.
34 H. Uedaira and H. Uedaira, *J. Solution Chem.*, 1985, **14**, 27–34.
35 Y. Zeng and D. J. Harrison, *Anal. Chem.*, 2007, **79**, 2289–2295.
36 E. L. Cussler, *Diffusion: Mass transfer in fluid systems*, Cambridge University Press, 2009.
37 V. Sourjik and H. C. Berg, *Proc. Natl. Acad. Sci. U. S. A.*, 2002, **99**, 123–127.
38 N. Vladimirov, L. Lovdok, D. Lebiedz and V. Sourjik, *Plos Computational Biology*, 2008, 4.
39 K. Yamamoto and Y. Imae, *Proc. Natl. Acad. Sci. U. S. A.*, 1993, **90**, 217–221.
40 R. W. Kasinskas and N. S. Forbes, *Biotechnol. Bioeng.*, 2006, **94**, 710–721.
41 R. R. Aksamit, B. J. Howlett and D. E. Koshland Jr., *J. Bacteriol.*, 1975, **123**, 1000–1005.
42 R. R. Aksamit and D. E. Koshland, *Biochemistry*, 1974, **13**, 4473–4478.
43 P. G. Strange and D. E. Koshland Jr., *Proc. Natl. Acad. Sci. U. S. A.*, 1976, **73**, 762–766.
44 M. Fahnestock and D. E. Koshland Jr., *J. Bacteriol.*, 1979, **137**, 758–763.